The rupture force of liquid bridges in two and three particle systems

Diana Lievano, Sachin Velankar, Joseph J. McCarthy*

Department of Chemical and Petroleum Engineering, University of Pittsburgh, Pittsburgh, PA 15261, USA

ARTICLE INFO

ABSTRACT

The measurement of the rupture force for an axially strained liquid bridge has been the subject of research for the last three decades and is fundamental to the understanding of the behavior of multiphase systems in granular materials. The study herein presents experimental work measuring the rupture force of pendular and capillary bridges in a three-particle configuration providing an axial and a shear strain. Results and subsequent analysis indicates that the rupture force and maximum rupture distance are the effect of surface characteristics, straining mechanism and effective liquid volume. For systems of more than two particles, we note that the effective packing fraction of the particles has a significant impact on the force required to rupture such a bridge.

© 2017 Elsevier B.V. All rights reserved.

1. Introduction

Investigating the phenomena involved in solid–liquid interactions is important due to the ubiquitous presence of compound solid–liquid systems among a variety of industries (i.e. pharmaceutical, chemical, cosmetic, and agricultural) and with diverse chemical and physical applications, such as agglomeration, and crystal growth. In these systems strong adhesion can result from the liquid meniscus that forms around the point of contact between solid surfaces [1]. This force is called the capillary force. In a two-particle system, these menisci bind solid surfaces by creating a bond between two finite contact points. The phenomenon of capillary adhesion is of great importance for granular materials and powders in the macroscale [2]. While the formation of agglomerates is commonplace in the industrial processing of solid mixtures, axial straining of a liquid bridge, in particular, can be evidenced in the granulation process.

Understanding and modeling multiphase systems is complex due to the different forces acting on the solids depending on the volume of fluid present. Depending on the liquid volume-capillary, surface and viscous forces can appear and change the mechanical properties of the mixture, such as its tensile strength [3–5]. The increasingly intricate interactions between the solid and liquid components, as the saturation level increases, has limited most of the

available experimental studies to the pendular regime, and analytical models are developed for stable pairwise, axisymmetric bridges. Furthermore, the study of the formation and rupture of binding liquid networks has the added problem of bridge stability, particularly when dealing with bridges linking spherical solids. To forgo this problem most studies are limited to working with *small* liquid volumes (relative to particle size) such that a stable meniscus can be sustained between the solids [6,7]. A formal definition of what we consider to be small liquid volumes will be discussed later.

The attraction or repulsion forces between solids and the interstitial liquid are a result of a pressure differential across the interface. The pressure differential can be calculated using the Young–Laplace (YL) equation if the shape of the meniscus is known [2]. Megias-Algacil & Gauckler [8,9] recently presented a study for the capillary forces between spheres for liquid volumes forming both concave and convex liquid bridges. The results analyze the nature of the cohesive forces and present values for contact angle and relative liquid volume, defined as $V_{rel} = V/\left(\frac{4}{3}\pi R^3\right)$, for which a concave or convex meniscus can be expected. Urso et al. [10,11] present theoretical two-dimensional studies for the rupture of liquid bridges including the transitional states between pendular and capillary saturation level. They introduce equations to calculate the area of the liquid bridge surface for different saturation states and meniscus geometries. Murase et al. [12,13] presented a first attempt at characterizing the straining phenomena for a liquid bridges of different volumes held between three spheres both experimentally and computationally. They focused largely on the differences between dynamic and

* Corresponding author.
E-mail address: jjmcc@pitt.edu (J.J. McCarthy).

static pendular bridge forces and conclude that the maximum tensile force of the liquid bridge is the same for the two and three sphere system for a static rupture mechanism, but two times larger for the three-particle configuration under dynamic rupture conditions.

It is the objective of this study to perform experimental measures for the rupture force of menisci between two- and three-sphere interactions. We will follow the taxonomy described by Urso et al. [10,11], where bridges between two particles are termed pendular, systems where the particle interstices are fully saturated are called capillary, and intermediate saturations where there are varying degrees of interstitial voids are considered to represent funicular saturation. This work will measure both pendular and capillary rupture forces with a focus on the impact of bridge volume and particle symmetry effects.

1.1. The rupture of a pendular liquid bridge

The rupture force for pendular liquid bridges has been studied for decades [2,4,5,14-18]. Particle–plane and particle–particle interactions have been modeled for spherical particles and small liquid volumes. In general, the solution to the rupture energy of a liquid bridge can be found by considering it as a two-part problem. First, the stability problem and second, the net attraction/repulsion forces induced by the formation of liquid bridges [4].

When considering a packed bed, the theory for different saturation levels identifies the limit of the pendular regime at ≈13% moisture content, while the funicular regime is identified as corresponding to a moisture content above 13% and up to 25% [19]. It is known additionally, that for small enough volumes, where the effect of gravity can be neglected, the mean curvature of the bridge surface between two spheres may be approximated as constant and the contact point is fixed [20]. The maximum volume of fluid, for which the effects of gravity can be considered negligible, is estimated using the following equation:

$$\kappa = \sqrt{\frac{\sigma}{g\rho}}, \tag{1}$$

where ρ_l is the density difference between the solid and the liquid phases, and κ is known as the capillary constant, or capillary length.

In order to model such interactions it is necessary to solve the Young–Laplace (YL) equation for capillary forces in the presence of a curved liquid-vapor interface. The pressure differential across the liquid-gas interface, is defined by the shape of the meniscus. It is commonplace to assume the shape of the meniscus is described by a solid of revolution [21]. While numerical solutions for the YL equation for a wide variety of revolution surfaces are known, more often than not, an equation based on a toroidal shape is implemented [7,22,23]. Based on this approach, in order to perform an axially oriented force balance, first a system in equilibrium is defined (Fig. 1). Then, making use of the surfaces of revolution to calculate the pressure differential across the liquid–gas interface according to YL, one employs the theories of capillarity and lubrication to calculate the total cohesive force [24,25].

The work discussed herein follows the procedure described by Pitois et al. for the rupture energy of a pendular liquid bridge [24]. The simplified dimensionless expression derived for the capillary force contribution takes the form

$$F^*_{cap} = \frac{F_{cap}}{\sigma R} = 2\pi \cos \phi \zeta_v, \tag{2}$$

with,

$$\zeta_v = 1 - \left(1 + \frac{(2V^*)}{(\pi D^{*2})}\right)^{\frac{-1}{2}}, \tag{3}$$
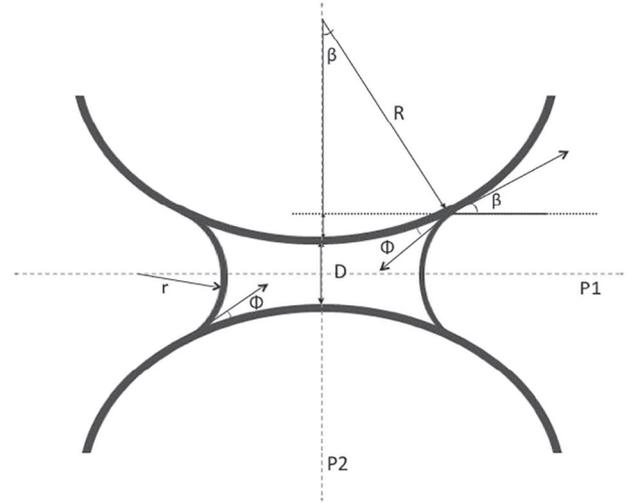

Fig. 1. Sketch of a liquid bridge formed between two spheres. P1 and P2 are planes of symmetry.

where D is the distance between the two solid surfaces, σ is the fluid surface tension, and ϕ is the solid-liquid wetting angle. The star symbol (*) denotes the dimensionless form of an expression. The length scale to write dimensionless parameters is the radius of the sphere R, such that $V^* = V/R^3$, $D^* = D/R$. Similarly, we use as the force scale σR (see Eq. (2)).

1.2. Viscous forces

An expression for the viscous force contributions to granular systems was developed by Ennis et al. based on a derivation of the Reynolds equation to describe thin film behavior [7]. The function revealed how the contribution of lubrication forces to the total rupture force becomes increasingly important for high viscosity fluids. While the objective of the current work is focused on low viscosity fluids only, we have implemented the viscous contribution as part of the computational model for completion. The viscous contribution, in its dimensionless form, can be written as:

$$F^*_{visc} = \frac{3}{2}\pi \frac{C_a}{D^*} \zeta_{v^2} \tag{4}$$

where, Ca is the capillary number defined as $C_a = \mu\sigma/a$, and μ is the viscosity of the fluid. It follows that the total (dynamic) force is the sum of the capillary and viscous terms. A relationship between the liquid bridge volume, the liquid–solid contact angle and the quasi-static rupture distance, was presented by Lian et al. [22] for liquid volumes where the effect of gravity can be neglected. Their rupture distance can be written as:

$$D^*_{rupt} \simeq \left(1 + \frac{\phi}{2}\right) V^{*1/3}. \tag{5}$$

The total liquid bridge force contribution can then be expressed as:

$$F^*_{tot} = 2\pi \cos \phi \zeta_v + \frac{3}{2}\pi \frac{C_a}{D^*} \zeta_v^2 \tag{6}$$

Key contributors to viscous forces, such as wetting angles, and stability on curved surfaces have become areas of independent studies [26–28]. Results indicated that minimal shifts in the shape of the meniscus had a significant impact on the evolution and rupture of the bridge. The present work will be concerned with steady state, non-thermodynamic equilibrium, and will assume the bridge

maintains a constant mean-curvature. Adams et al. [29] present a study on mapping the influence of gravitational forces for the liquid binding of solid spheres. The Bond number (Bo) – defined as $Bo = \Delta\rho g d^2/\sigma$ where d is the characteristic length – is used to quantify the gravitational distortion for a free liquid droplet. It serves as a characterization parameter when a scaling factor – which is a function of the liquid bridge volume (V) – is introduced. The modified Bond number is defined as V^*Bo and was used in Ref.[29] to predict the influence of gravitational forces. In this work, Adams et al. identified systems that have $V^*Bo < 0.01$ as being essentially gravity free, while systems in the range $0.01 < V^*Bo < 0.015$ are deemed transitional and those with $V^*Bo > 0.015$ are the considered to be gravity controlled systems (that is, they are systems in which the gravity component plays a significant role in the meniscus evolution and subsequent bridge rupture). For axisymmetric pendular rings between a sphere with radius R and a flat surface, the Bond number is expressed as $Bo = \Delta\rho g R^2/\sigma$ where the characteristic length is the particle radius. For while for a liquid bridge between identical spheres, on the other hand, the Bond number can be expressed in terms of the liquid volume (V), as:

$$Bo = \Delta\rho g V/R\sigma. \tag{7}$$

When the largest dimension of a sessile drop exceeds κ the gravitational effects become significant, and the straining of a liquid bridge (between two spheres) produces a decrease in the liquid filling angle (β) of the top sphere as separation increases (see Fig. 1) until eventually the bridge becomes unstable. For these cases, Adams et al. suggest a modified rupture criterion of the form

$$D^*_{rupt} \simeq (1 - 0.48V^*Bo)V^{*1/3}. \tag{8}$$

2. Materials & methods

Rupture tests were performed using acrylic beads of 2 mm in diameter. Ethylene-glycol (EG) was selected as the fluid to minimize evaporation at ambient conditions (refer to Table 1 for relevant fluid properties). Different fluid volumes were tested in order to describe the relationship between liquid volume and rupture behavior in the pendular and capillary regimes.

2.1. Measurement of micromechanical forces in an axially strained liquid bridge

To measure the rupture forces of liquid binding networks, a micro-mechanical force microscope was constructed, which consists of a (Philtec) fiberoptic sensor, a stainless-steel cantilever and a moving stage. Data is collected and interpreted using two essential components: (1) a multi-purpose texture analyzer (Brookfield Engineering), and (2) a DMS optical displacement sensor. The two devices are coupled via a stainless-steel cantilever (thickness = 0.007 inches), see Fig. 2. The fiberoptic sensor can be programmed to

Table 1
Properties for ethylene glycol at 20 ° C.

Property	Value	Units
Molar mass	62.07	g/mol
Density	1.11	g/cm^3
Viscosity	0.015	Pa s
Surface tension	0.048	N/m
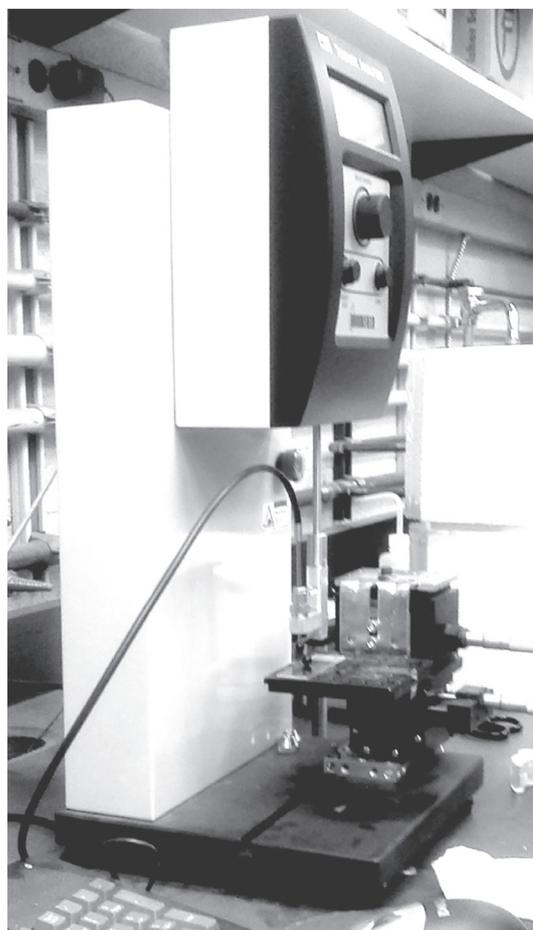
Fig. 2. Micromechanical force microscope: Brookfield texture analyzer casing, stainless-steel retractible cantilever, optical displacement sensor.

translate the reflectivity measurement to a distance and is calibrated in-situ. The reflectivity itself is a function of the cantilever properties as well as the finished surface.

The texture analyzer (TA) holds the stage for the static bottom particle(s), as well as the retractable shaft, which is fitted with a custom stainless-steel cantilever. A retracting particle – identical to the stationary one(s) – is fixed to the underside of the distal end of the cantilever. This sphere cantilever unit is the sole mobile element in this setup, which simultaneously imparts axial strain on liquid bridges and measures the force between the particles within the system. Directly above and parallel to the cantilever is an arm which holds the optical displacement sensor. As the shaft is raised, liquid forces operating on the retracting sphere bend the cantilever from its resting position. As the distance between the cantilever and the optical sensor changes, the reflectivity of the cantilever beam is altered and this change is calibrated to yield a strain (length). Based on the measured bending modulus of the cantilever, this strain is converted to a force. The choice of cantilever thickness is determined via trial-and-error in which different thicknesses impact the accuracy of force measurement (due primarily to a changing signal-to-noise ratio). In practice, we base our selection of cantilever on a calibration of the strain to force conversion over the entire range of interest. The particle, cantilever and sensor configuration is displayed in Fig. 2.

The retraction velocity employed must ensure slow displacement of the cantilever such that the rupture is considered quasi-static. The TA device allows setting the shaft displacement at 10 μm/s, a velocity slow enough to capture the static rupture as indicated in Fig. 4.

The optical sensor software keeps a real-time record of the reflectivity as well as the distance between the sensor tip and the cantilever surface. Having a set, constant shaft-speed allows for the straightforward calculation of the distance displaced in time. A qualitative analysis of the primary experimental measurements is performed in order to validate that the shaft operating velocity used in this work is slow enough to approximate quasi-static operation. The rupture of a liquid bridge under dynamic conditions is beyond the scope of the current work.

Making use of Eqs. (1) and 5, inserting the corresponding values for gravity and EG properties (i.e. density, surface tension, see Table 1), we calculate the rupture distance and relate it to the particle volume proposed by Lian et al. [22]. A gravity free liquid bridge corresponds to effective volumes where $V^{*1/3} < \kappa$, following the rationale presented in Eq. (1) [1]. Therefore, for the particles used in this study the maximum volume allowable in order to correctly neglect gravitational forces is ≈0.5 μL. This calculated volume highlights the importance of operating with small particles. Operating with liquid volumes above 0.5 μL could give rise to non-negligible gravitational forces [22].

2.2. Experimental methodology

Each run is initiated in the same manner; a drop of volume *V* is carefully dispensed with a syringe on top of the bottom sphere(s), which remain static. The cantilever sphere is then slowly brought into contact first with the liquid drop(s) then with the opposing particle surface(s). After contact with the drop(s), the liquid is displaced to the surface surrounding the contact spot(s). The instant the top bead starts retracting by action of the shaft, the fluid will make its way into the newly available gap and produce the peak force reading in the force distance diagram. In the case of three-particle interactions, drops of EG – comprised of varying volumes – are applied to the top surfaces of each static bead, such that when the cantilever sphere is lowered, a liquid bridge conjoins all particles (either with one large capillary bridge or two (separate) pendular bridges). As before, prior to the start of each trial, the top and bottom beads are positioned in direct contact.

The data is herein presented in dimensionless terms, unless stated otherwise. Terms will be made dimensionless by using the particle radius, and surface tension of the fluid, ethylene glycol (EG).

3. Results and analysis

In the interest of verifying the accuracy of the measurements recorded by the micro-mechanical force microscope, initial tests were aimed at validating the experimental methodology. Accordingly, the rupture force for a single pendular liquid bridge was measured for a sphere-plane configuration. Fig. 4 presents the tensile strength behavior between a glass plate and a sphere measured experimentally and compared to the corresponding theoretical function as a function of the separation between particles *D*. For all force curves presented herein, the last point plotted represents the maximum separation achieved before rupture occurred.

The theoretical curves shown in Fig. 4 were plotted following the analysis presented by Pitois et al. which calculates the quasi-static adhesive force for a constant liquid bridge volume with pinned contact points (refer to Eqs. (2) and 4; [25]). The fluid properties of EG were used in the theoretical calculations. The total force data appears to lie on the same curve as the capillary force equation (Fig. 3), which supports that capillary, not viscous, forces dominate in this system. Throughout the range of particle separation the measured data falls within two standard deviations (based on five independent trials) from the theoretical curve. The agreement observed between the
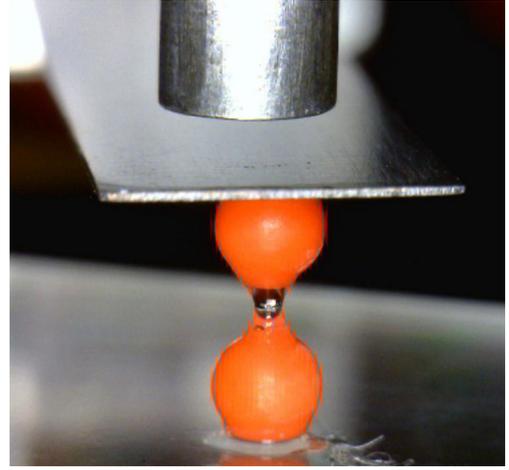

Fig. 3. Image of a pendular liquid bridge between two spheres. The top sphere is attached to the cantilever and the bottom sphere is held static. Straining of the liquid bridge is a result of the upwards movement of the top sphere at constant speed.

measured and theoretical curves lends validity to the assumption that our experimental setup accurately approximates static operation. It is accepted from here on that measurements taken employing this methodology and operational parameters correspond to quasi-static behavior of the liquid system and the term will be omitted for the sake of brevity.

In addition to this, for the widely studied plate and sphere system, the rupture distance obtained experimentally follows the relation predicted by Lian et al. [22], Eq. (5). The selection of EG as the fluid has the advantage of displaying contact angles close to zero, therefore assuming $\phi = 0$ for all systems the above expression reduces to

$$\tilde{D}_{rupt} \approx V^{*\,1/3} \qquad (9)$$

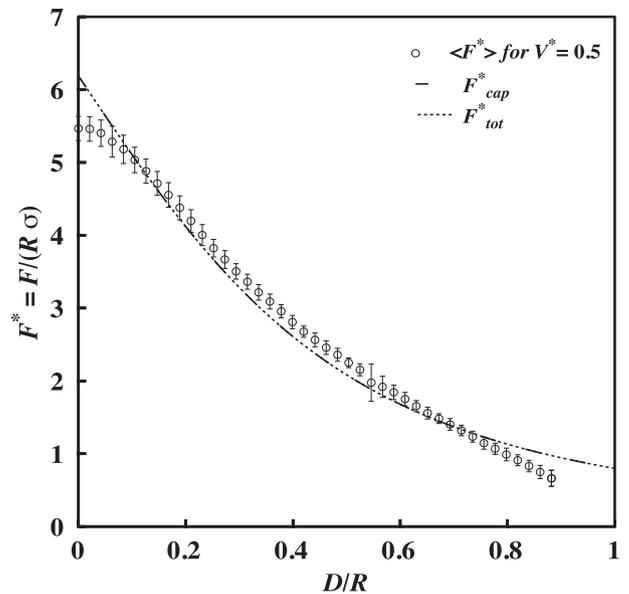which underestimates the rupture distance observed in Fig. 4 by 11%.

Fig. 4. Quasi-static force between an acrylic sphere and glass plane forming a pendular liquid bridge measured experimentally compared with the calculated theoretical values for F_{cap}^* (Eq. (2)), and F_{tot}^* (Eq. (6)) as described by Pitois et al. The fluid used is ethylene glycol.

Table 2
Properties for ethylene glycol at 20 ° C.

Target V^*	V^*Bo	$V^{*1/3}$	D^*_{rup} (gravitational mapping)
0.25	0.057	0.63	0.63
0.50	0.11	0.79	0.75
0.75	0.17	0.90	0.83
1.0	0.23	1.0	0.89
2.0	0.45	1.3	0.98

3.1. Liquid bridges between two particles

Calculating the modified Bo number suggests that only dimensionless volumes above one (1) will exhibit gravity effects that affect the draining mechanism. Here, our use of the term draining mechanism refers to the observed retraction and redistribution of fluid as the liquid bridge is stretched (and ultimately ruptured). In the more simple particle-wall or 2-particle systems the draining mechanism is the same for all liquid volumes, being characterized by the formation of a (thinning) bridge neck at approximately $h = S/2$ as stretching occurs. When rupture occurs, the neck region breaks and there are two resulting droplets of similar volumes that remain at the contact point of both the top and bottom particle. For more complex systems with three particles and multiple liquid bridges the draining mechanism is dependent on the degree of symmetry of the initial condition, see Fig. 7. Table 2 presents values of liquid volume that are used in the experimental trials described in this section. According to the V^*Bo values calculated, we expect the liquid volumes $0.5 \leq V^* \leq 0.75$ to be in the transitional regime, where there is a significant decrease in the rupture distance and change in the force by half of the bridge weight. Similarly, for volumes where $V^* \geq 0.75$, we anticipate being in the gravity controlled regime. The expected rupture distances are also presented in the table based on Eqs. (9) or 8 (according to the expected gravitational regime).

According to the modified rupture distance approximation proposed by Adams et al. the gravitational effects reduce the rupture distance as much as 20% for the larger liquid volumes dispensed.

In order to observe the sensitivity of the measurements, the results for three characteristic runs are plotted for each (liquid volume) condition. The two-particle bridge rupture results presented in Fig. 5 are further supported by other indicators reported in literature. Most notably, the maximum force is about half of the sphere-plane rupture force [1], for the same liquid volume.

The measured tensile force of the liquid bridge is in accordance with theoretical values presented by Willett et al. [17] where the maximum capillary force is considered insensitive to the liquid volume for pendular bridges, without gravity effects. In addition to this, Willet et al. reported rupture distances being overestimated by Eq. (5), and suggested an alternate best-fit solution of the form:

$$D^*_{rupt} = \left(1 + \frac{\phi}{2}\right)\left(V^{*1/3} + \frac{V^{*2/3}}{10}.\right) \tag{10}$$

Results presented in Fig. 5 also support this observation, as the expected rupture distances are underestimated by Eqs. (9) and 8, whereas the modified expression presented by Willet et al. describes accurately the results presented for two particles.

3.2. Three particle system and capillary liquid bridges

When testing a three-particle set-up, two different configurations were used: one simulating a high solid fraction — where particles are closer together; and one simulating a low solid fraction — where the stationary particles are separated. A setup with a center-to-center distance between the two bottom spheres of $d^* = d/R = 2.5$ was chosen as the high solid fraction condition, to test a triple contact starting point. The initial condition for the force measurement is when the drop is in contact with all three spheres. The results for three different *effective* liquid volumes are presented in Fig. 6.

Contrary to the experimental results presented in Murase et al. [12] the observed trend for the force of a single liquid bridge in contact with three spheres (Fig. 6) does not result in the same maximum
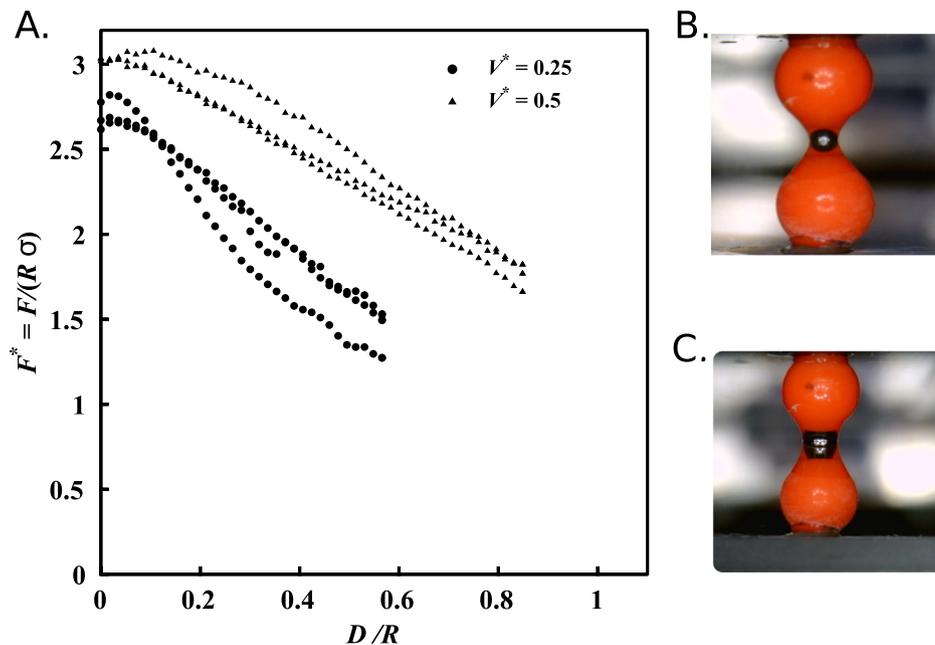
Fig. 5. A) Experimentally measured capillary force versus separation curves for an axially strained pendular liquid bridge formed between two identical acrylic spheres ($R = 1$ mm). Three runs for each corresponding liquid volume ($V^* = 0.25$, $V^* = 0.50$) of ethylene glycol are presented. B) Picture liquid bridge of volume $V^* = 0.25$. C) Picture liquid bridge of volume $V^* = 0.50$.

A.

B.

C.
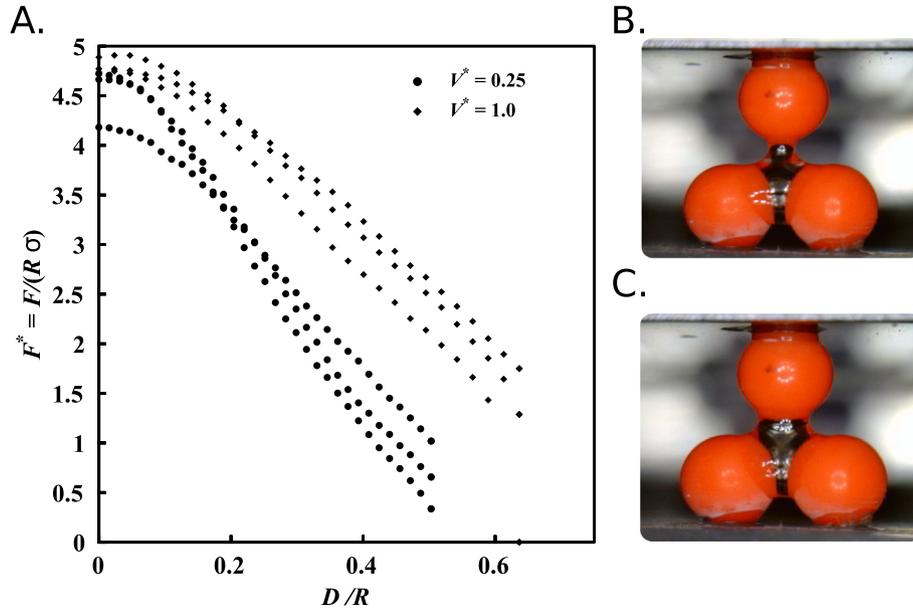
Fig. 6. A) Measured liquid bridge force for a single axially strained bridge in contact with three identical acrylic spheres. Three runs are plotted for each of the liquid volumes used ($V^* = 0.25$, $V^* = 1.0$). The center-to-center distance for the bottom spheres is $d^* = 2.5$. B) Picture liquid bridge $V^* = 0.25$. C) Picture liquid bridge $V^* = 1.0$.

capillary force as it does for two spheres (Fig. 5). In fact, the maximum measured force is higher when the liquid bridge is stretched over three particles, where we obtain a value comparable with the maximum force for a liquid bridge between a sphere and a plane. This can be explained by the fact that the liquid volume distributes among the two bottom spheres creating a meniscus with a shape closer to that formed between a sphere and a plane.

The rupture distance, on the other hand, is reduced by about 20% for the gravity-free volume of $V^* = 0.25$, and is roughly half the expected length for the capillary saturation volume of $V^* = 1.0$, indicating that rupture distance approximations are only applicable for pendular liquid bridges.

We should note that, for capillary saturation volumes, imprecise draining mechanisms were observed for some of the runs. During these runs the liquid meniscus shifts forming a two-particle bridge between the cantilever sphere and only one of the static beads. In the most frequently seen draining mechanism, a single bridge forms as it does between two spheres, yet the neck of the meniscus forms closer to the top sphere allowing the majority of the volume to be balanced between the bottom two (see Fig. 7).

The second configuration tested was that mimicking a low solid fraction particle bed, meaning there is a greater gap between adjacent spheres. Again, two drops are dispensed – one above each of the bottom spheres – which now lay at a measured center-to-center distance of $d^* = 3.2$, Fig. 8B and C. The cantilever is lowered until the top sphere makes contact with the two bottom spheres without allowing the two drops to coalesce. For these cases the liquid volume reported corresponds to the liquid volume *per bridge*, meaning the total liquid volume of the system is twice as much.

The maximum force for two liquid bridges held in a three-particle configuration presents two noteworthy characteristics. First, the maximum force is larger than that of a single liquid bridge held between two spheres. A way to understand this is to think of two springs in parallel. Two identical springs in parallel exert a force that is effectively twice the force of a single bridge, Fig. 9A; however, when these springs are inclined at an angle (θ) the force is reduced by a factor of $\sin\theta$, as in Fig. 9B. For the configuration used in our experimental trials the true angle between the particle centers is approximately $\theta = 50°$; however, using this correction overestimates the degree to which the maximum bridge force increases, perhaps
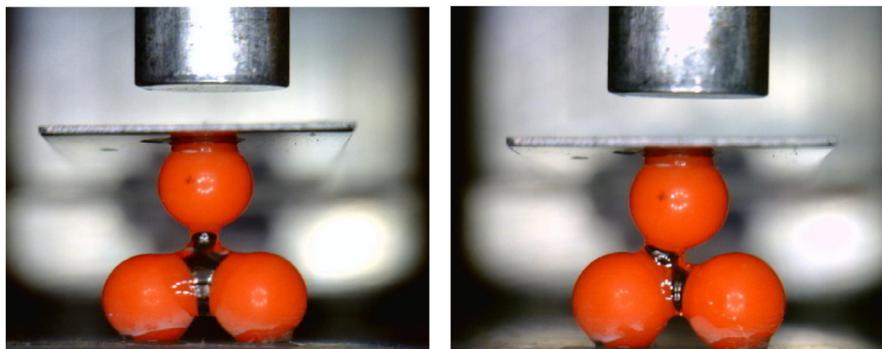

Fig. 7. Comparison of the two primary draining behavior observed for a single bridge between three identical spheres. Left: Axially strained single bridge where the neck of the meniscus is located closer to the top sphere. Right: Asymmetrical draining and rupture of the meniscus.
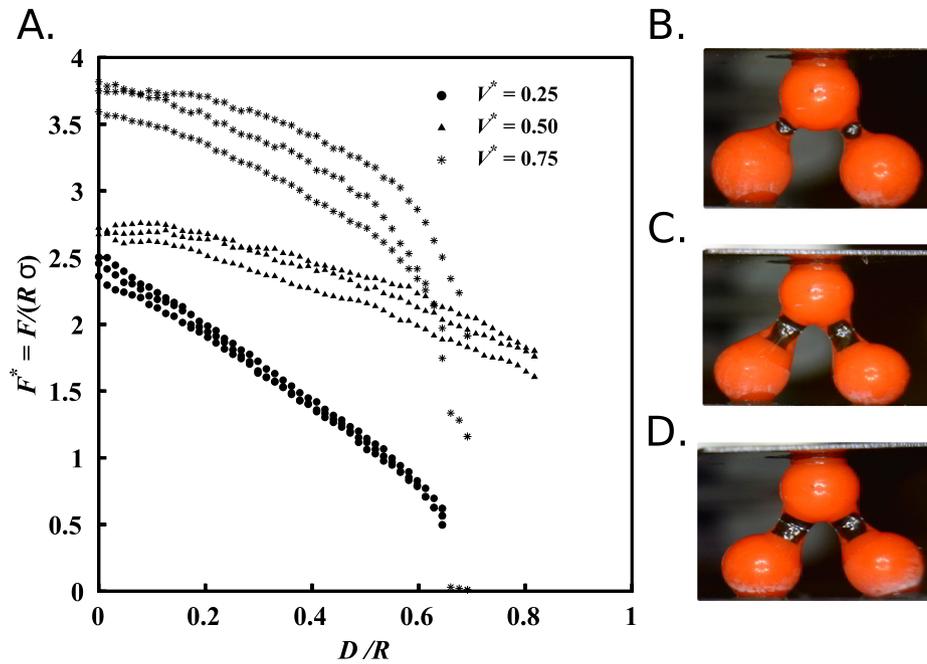
Fig. 8. A) Measured capillary force between for two axially strained liquid bridges formed between three identical spheres. Two separate drops are initially placed on top of each of the bottom spheres. Three runs are plotted for each of the liquid volumes used ($V^* = 0.25$, $V^* = 0.50$, and $V^* = 0.75$). The center-to-center separation between the bottom particles is $d^* = 3.2$. B) Picture liquid bridge $V^* = 0.25$. C) Picture liquid bridge $V^* = 0.50$. D) Picture liquid bridge $V^* = 0.75$.

due to interactions between the wetted contact spots on the central particles. Second, the maximum force is seen to increase with
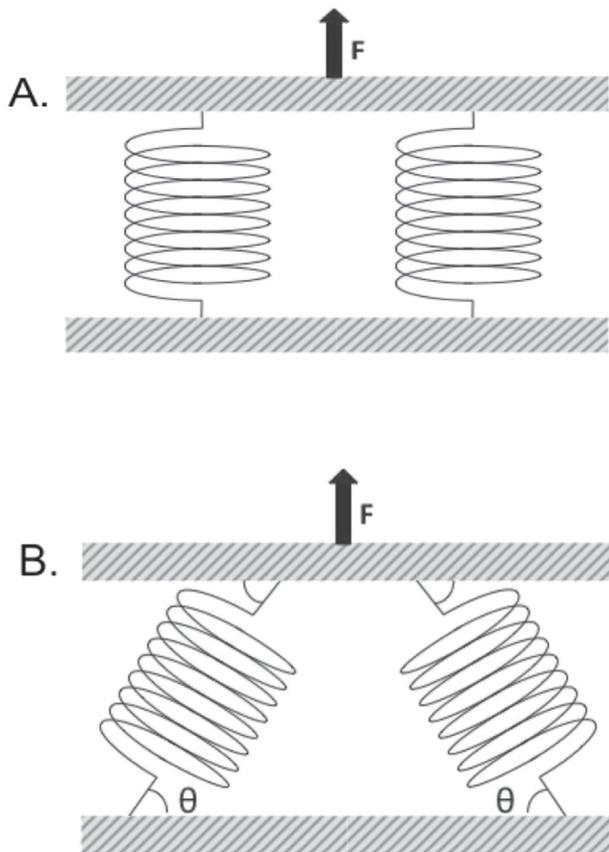
Fig. 9. Parallel between the combined effect of two springs in parallel and two liquid bridges held between a three particle unit. A) Shows to springs stretched normal to the surface B) Two springs stretched at an angle θ with respect to the surface.

increased liquid volume, despite the presence of pendular bridges, ostensibly in contrast to the findings of Willett et al. [17] (and our results in Fig. 5). We believe that this can be explained as a consequence of two factors: as the liquid volume increases, the effective angle observed between the bridges decreases (thus the factor of $\sin\theta$ increases); additionally, the increased liquid volume is large enough to set our results into the transitional gravitational regime (where liquid volume is expected to affect the maximum force observed).

The rupture distance for this case is similar to that of the two-particle configuration, and is approximated to a good degree by Eq. (10) for $V^* = 0.25$ and $V^* = 0.5$. For $V^* = 0.75$ the rupture distance is better predicted by the modified rupture proposed by Adams et al., for liquid bridges in the transitional regime, indicating the latent effect of gravitational forces for this volume.

Finally in Fig. 10, we compare the rupture force for a dispensed volume of $V^* = 2.0$ distributed among two or three particles. Interestingly, for these large liquid volumes we still don't perceive a significant reduction of the maximum capillary force due to gravitational effects. They do, however, exhibit a reduction in the rupture distance that is more significant for the three-particle system than it is for the two-particle configuration. In addition to this, the maximum force is comparable between the close-packed three-particle and the plate-sphere configuration. This can be explained by observing the meniscus shape for both systems, where a single drop in contact with three spheres creates a meniscus geometry that more closely resembles that formed between a sphere and plate. From a qualitative standpoint, our results are also in agreement with Urso et al. [11] in that a pendular configuration will allow for a larger rupture distance than the corresponding capillary configuration, while the latter has a larger maximum binding force.

4. Summary and conclusions

In the present study, we measure the quasi-static rupture force of pendular and capillary liquid bridges by using a micro-mechanical
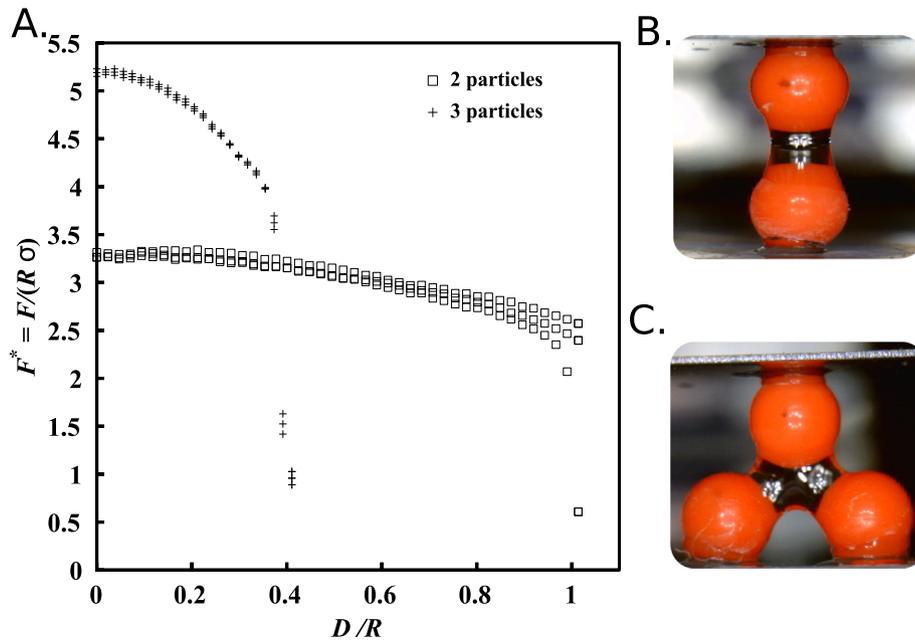
Fig. 10. A) Rupture force for a dispensed liquid volume $V^* = 2.0$ in a 2 sphere and 3 sphere setup. The three-particle configuration here corresponds to the low solid fraction with $d^* = 3.2$. Three runs are plotted for the two and three particle configuration. B) Picture of liquid bridge ($V^* = 2.0$) held between two particles. C) Picture of liquid bridge ($V^* = 2.0$) held between three particles.

force microscope comprised of a Brookfield TA and a fiber optic sensor. We find that the maximum tensile energy of capillary liquid bridges varies with drop volume, contact angle and bridging/draining mechanism. In particular the degree of symmetry of the initial condition was found to have a significant effect on the contact angle, the bridging/draining mechanism and ultimately the maximum liquid volume which forms a stable liquid bridge. To our knowledge, this observation is reported here for the first time.

As another unique focus of the present work, we examine the impact of interparticle spacing on the strength of bridge force networks. We note that capillary liquid bridges are capable of forming strong binding networks given a close packed granular system, but that these networks significantly decrease in strength as the particle spacing grows (and the same saturation level now leads to individual, pendular bridges). These observed trends in F^* suggest that closely packed granular systems could display a higher cohesion effect than what would be expected based on two-particle system theory. Observations presented here indicate an increase of anywhere between 28 and 67% for F^* when the liquid bridge extends between three spheres when compared to the two sphere system depending on the proximity of the particles and the liquid volume. While this effect needs to be studied further it is our hypothesis that this is the result of the meniscus geometry. For closely packed granules and high fluid volumes, the base spheres could approximate the effect of a bottom flat surface resulting in a net increase in the maximum force. This hypothesis could be validated by measuring liquid bridge forces formed between planes of spheres with varying packing fractions.

References

[1] H.-J. Butt, M. Kappl, Adv. Colloid Interf. Sci. 146 (1-2) (Feb 2009) 48–60.
[2] P.C.T de Boer, M.P de Boer, Rupture work of pendular bridges, Langmuir: the ACS J. Surfaces Colloid 24 (1) (Jan 2008) 160–169.
[3] P. Pierrat, H.S. Caram, Tensile strength of wet granular materials, Powder Technol. 91 (1997) 83–93.
[4] C.L. Feng, A.D. Yu, Effect of liquid addition on the packing of mono-sized coarse spheres, Powder Technol. 99 (1) (Sep 1998) 22–28.
[5] Y.I. Rabinovich, M.S. Esayanur, B.M. Moudgil, Capillary forces between two spheres with a fixed volume liquid bridge: theory and experiment, Langmuir: ACS J. Surf. Colloids 21 (24) (Nov 2005) 10992–10997.
[6] K. Hotta, K. Takeda, K. Iinoya, The capillary binding force of a liquid bridge capillary, Powder Technol. 10 (1974) 231–242.
[7] B.J. Ennis, J. Li, G. Tardos, R. Pfeffer, The influence of viscosity on the strength of an axially strained pendular liquid bridge, Chem. Eng. Sci. 45 (10). (1990) (3071–2088).
[8] D. Megias-Alguacil, L.J. Gauckler, Capillary forces between two solid spheres linked by a concave liquid bridge: regions of existence and forces mapping, AIChE J. 55 (5). (2009).
[9] D. Megias-Alguacil, L.J. Gauckler, Analysis of the capillary forces between two small solid spheres binded by a convex liquid bridge, Powder Technol. 198 (2) (Mar 2010) 211–218.
[10] M.E. Urso, C.J. Lawrence, M.J. Adams, Pendular, funicular, and capillary bridges: results for two dimensions, J. Colloid Interface Sci. 220 (1) (Dec 1999) 42–56.
[11] M.E.D. Urso, C.J. Lawrence, M.J. Adams, A two-dimensional study of the rupture of funicular liquid bridges, Chem. Eng. Sci. I (2002) 677–692.
[12] K. Murase, T. Mochida, H. Sugama, Experimental and numerical studies on liquid bridge formed among three spheres, Granul. Matter 6 (2-3) (Oct 2004) 111–119.
[13] K. Murase, T. Mochida, Y. Sagawa, H. Sugama, Estimation on the strength of a liquid bridge adhered to three spheres, Adv. Powder Technol. 19 (4) (Jun 2008) 349–367.
[14] W.C. Clark, J.M. Haynes, G. Mason, Liquid bridges between a sphere and a plane, Chem. Eng. Sci. 23 (Table 1) (1968) 810–812.
[15] H. Schubert, Capillary forces — modeling and application in particulate technology, Powder Technol. 37 (1984) 105–116.
[16] S.J.R. Simons, J.P.K. Seville, M.J. Adams, An analysis of the rupture energy of pendular liquid bridges, Chem. Eng. Sci. 49 (14) (1994) 2331–2339.
[17] C.D. Willett, M.J. Adams, S.A. Johnson, J.P.K. Seville, Capillary bridges between two spherical bodies, Langmuir 16 (24) (2000) 9396–9405.
[18] J.-P. Gras, J.-Y. Delenne, M.S. El Youssoufi, Study of capillary interaction between two grains: a new experimental device with suction control, Granul. Matter 15 (1) (Dec 2012) 49–56.
[19] C.L. Flemmer, On the regime boundaries of moisture in granular materials, Powder Technol. 66 (1991) 191–194.
[20] F.M. Orr, L.E. Scriven, A.P. Rivas, Pendular rings between solids: meniscus properties and capillary force, J. Fluid Mech. 67 (04) (Mar 1975) 723.
[21] S.J.R. Simons, J.P.K. Seville, M.J. Adams, An analysis of the rupture energy of pendular liquid bridges, Chem. Eng. Sci. 49 (14) (1994) 2331–2339.
[22] G. Lian, C. Thornton, M.J. Adams, A theoretical study of the liquid bridge forces between two rigid spherical bodies, J. Colloid Interface Sci. 161 (1993) 138–147.

[23] B.Y. Rubinstein, L.G. Fel, Theory of axisymmetric pendular rings, J. Colloid Interface Sci. 417 (Mar 2014) 37–50.
[24] O. Pitois, P. Moucheront, X. Chateau, Liquid bridge between two moving spheres: an experimental study of viscosity effects, J. Colloid Interface Sci. 231 (1) (Nov 2000) 26–31.
[25] O. Pitois, P. Moucheront, X. Chateau, Rupture energy of a pendular liquid bridge, Phys. J. B 86 (2001) 79–86.
[26] S.F. Chini, A. Amirfazli, A method for measuring contact angle of asymmetric and symmetric drops, Colloids Surf. A Physicochem. Eng. Asp. 388 (1–3) (Sep 2011) 29–37.
[27] M. Soleimani, R.J. Hill, T.G.M. van de Ven, Bubbles and drops on curved surfaces, Langmuir: ACS J. Surf. Colloids 29 (46) (Nov 2013) 14168–14177.
[28] H.B. Eral, D.J.C.M.T. Mannetje, J.M. Oh, Contact angle hysteresis: a review of fundamentals and applications, Colloid Polym. Sci. 291 (2) (Sep 2012) 247–260.
[29] M.J. Adams, S.A. Johnson, J.P.K. Seville, C.D. Willett, Mapping the influence of gravity on pendular liquid bridges between rigid spheres, Langmuir 18 (16) (2002) 6180–6184.